Visualizing ultrafast electron transfer processes in semiconductor-metal hybrid nanoparticles: towards excitonic-plasmonic light harvesting

Franco V. A. Camargo[1‡], Yuval Ben-Shahar[2,3‡], Tetsuhiko Nagahara[1,4], Yossef E. Panfil[2], Mattia Russo[1], Uri Banin[2], Giulio Cerullo[1]**

[1] Dipartimento di Fisica, IFN-CNR, Politecnico di Milano, Piazza Leonardo da Vinci 32, Milan, Italy

[2] Institute of Chemistry and Center for Nanoscience & Nanotechnology, The Hebrew University of Jerusalem, 91904, Israel

[3] Department of Physical Chemistry, Israel Institute for Biological Research, P.O. Box 19, Ness-Ziona 74100, Israel

[4] Department of Chemistry and Materials Technology, Kyoto Institute of Technology, Matsugasaki, Kyoto 6068585, Japan

Supporting information

Synthesis of CdSe Nanorods

CdSe NRs were synthesized using modification of a previously reported procedure employing quasi-one-pot synthesis using Cd- tetradecylphosphonic acid (TDPA) complex and multiple injections. In a typical synthesis, cadmium oxide (CdO; 0.138 g), TDPA (0.595 g) and trioctylphosphine oxide (TOPO; 2 g) were mixed in a 100 mL three-neck flask. The mixture was heated to 120 °C and placed under vacuum for 1 h before being heated at 300 °C under argon atmosphere. The mixture was kept at that temperature until all of the CdO dissolved and turned clear and colorless. The mixture was then allowed to cool to room temperature and aged overnight at a glovebox. The aged Cd mixture was heated to 120 °C and placed under vacuum for 1 h before purging it three times with argon. While under the argon atmosphere, the solution was heated to 350 °C. After reaching 350 °C, a solution of dissolved selenium powder (Se; 0.052 g) in tributylphosphine (TBP; 0.151 g), toluene (0.230 g) and trioctylphosphine (TOP; 1.1 g) was swiftly injected to the hot mixture. At that point, the temperature was reduced to 250°C for growth. A noticeable color change was usually observed 1 min after injection. A second solution of Se (0.26 g) dissolved in TOPO (2.04 g) and toluene (0.15 g) was prepared and added drop-wise over the course of 2 hours starting 20 min into the reaction after the initial injection. Following the second injection the mixture was left to stir for additional 4 hours. Next, the reaction was quenched by removing the heating mantle and cooling the mixture with a fan. The crude reaction mixture was then diluted with toluene. Lastly, methanol was added to the reaction mixture in order to precipitate the nanocrystals and remove excess surfactants.

Synthesis of CdSe:Au Hybrid Nanorods

The deposition of the Au domain on the CdSe NRs was conducted by a combination of two different synthetic strategies into a single procedure. In the first step, a precursor stock solution consisting of octadecylamine (ODA; 0.055 g), di-dodecylammoniumbromide (DDAB; 0.021 g) and $AuCl_3$ (0.015 mg) in toluene (10 mL) was sonicated for 15 min to dissolve the $AuCl_3$; the solution changes color from dark brown to yellow during this process. In order to achieve selective growth of 1.5–1.8 nm gold tips on the apexes of the NRs, a molar ratio ~2000 Au ions per NR was used depending on the specific properties of

the NRs. A diluted Au growth stock solution was added to CdSe NRs (~$2x10^{-9}$ mol) in toluene (20 mL) in a 50 mL flask under flowing argon. The solutions were mixed and left in the dark for 1 h at room temperature. The product hybrid nanoparticles (HNPs) were then washed, precipitated with acetone and separated via centrifugation. Next, a light-induced metal deposition step was performed. A mixture of small tipped CdSe-Au HNPs (typically ~$8x10^{-10}$ mol) in 10 mL of toluene was placed in an inert atmosphere and in a low temperature environment, ~2-4°C. Different Au^{3+}/NR molar ratios, around 10000 Au ions per NR, of the diluted Au growth stock solution were then added to the mixture; this addition was followed by illumination with a blue light-emitting diode (100 mW) for, typically, 30 min. This step resulted in the additional growth of the metal tip. The resulting HNPs were then washed and precipitated with acetone, followed by separation via centrifugation to obtain the final HNPs.

Phase transfer

To carry out the transfer of the NRs and HNPs to water, we employed ligand exchange and polymer coating methods. Polymer coating was done with Polyethylenimine (PEI). The nanoparticles solution (1 mL) was mixed with PEI (0.15 g; MW 25,000) in chloroform (1 mL) for 1 h. The particles were then precipitated and washed with cyclohexane (1:1 chloroform/cyclohexane), followed by centrifugation. Next, triple distilled water was added to the precipitate and residues of PEI were removed by centrifugation. Additionally, the polymer coated particles were washed through a 100 KDa cellulose membrane in order to remove any polymer residues in the water suspended nanoparticles.

Calculations

Transition energies calculation methodology: We have calculated the energy levels and the electron and hole wave-functions of the CdSe NRs using the multiphysics mode of COMSOL.[1,2] Electron and hole states are calculated with a 3D single-band effective mass Hamiltonian. For the hole, we have solved the effective mass Hamiltonian for the heavy-hole band (hh), light-hole band (lh) and split off band (so) independently, neglecting their mixing. We have also included the electron-hole Coulomb interaction by solving the Schrödinger-Poisson equations. The dimensions we used in the calculation are based on experimental data, 8.4 nm diameter and 25 nm length. Material-dependent parameters such as effective masses ($m^*_{e,h}(r)$) dielectric constants ($\epsilon(r)$), and conduction and valence band profiles ($V^{e,h}_{confinement}$) used in this calculation are summarized in Supplementary Table 1. The entire computational space extends further from the NR boundary allowing for electron and hole wavefunctions to extend outside of the NR boundaries and decay into free space.

We start the simulation by computing the non-interacting electron and hole states by solving the Schrödinger equation:

$$\left(-\frac{\hbar^2}{2}\nabla\left(\frac{1}{m^*_e(r)}\nabla\right)+V^e_c(r)\right)\Psi^n_e = E^n_e\Psi^n_e(r) \qquad (1)$$

$$\left(-\frac{\hbar^2}{2}\nabla\left(\frac{1}{m^*_{hh,lh,so}(r)}\nabla\right)-V^{hh,lh,so}_v(r)\right)\Psi^n_{hh,lh,so} = E^n_{hh,lh,so}\Psi^n_{hh,lh,so}(r) \qquad (2)$$

We use von Neumann boundary conditions at the outer boundaries of the CdSe NR in order to impose the Ben-Daniel-Duke condition. At the edge of the computational domain (around 100 nm away from the

NR) we set the Dirichlet boundary-condition by setting the wavefunction to zero. After normalization of the wavefunctions, the Poisson equation is solved to derive the hole or electron Coulombic potential generated from the other particle $\phi_{e,hh}(r)$ under the assumption that the electron (hole) sees on average the highest (lowest) energy wave-function of the hole (electron).

$$\nabla\left(\varepsilon_0 \cdot \varepsilon(r)\nabla\phi_e(r)\right) = -q_e\langle\Psi_e(r)|\Psi_e(r)\rangle \quad (3)$$

$$\nabla(\varepsilon_0 \cdot \varepsilon(r)\nabla\phi_{hh}(r)) = q_e\langle\Psi_{hh}(r)|\Psi_{hh}(r)\rangle \quad (4)$$

With these potentials, Schrödinger equations are solved again for the electron and the hole with all of the contributions to the potentials:

$$\left(-\frac{\hbar^2}{2}\nabla\left(\frac{1}{m_e^*(r)}\nabla\right) + V_c^e(r) + q_e \cdot \phi_{hh}(r)\right)\Psi_e^n(r) = E_e^n\Psi_e^n(r) \quad (5)$$

$$\left(-\frac{\hbar^2}{2}\nabla\left(\frac{1}{m_{hh,lh,so}^*(r)}\nabla\right) - V_v^{hh,lh,so}(r) - q_e \cdot \phi_e(r)\right)\Psi_{hh,lh,so}^n(r) = E_{hh,lh,so}^n\Psi_{hh,lh,so}^n(r) \quad (6)$$

The emission energy was calculated by:

$$E_{emission} = E_g + E_e^i + E_{hh,lh,so}^i - E_{coulomb} \quad (7)$$

$$E_{coulomb} = \frac{E_e^i - E_e^f + E_{hh,lh,so}^i - E_{hh,lh,so}^f}{2} \quad (8)$$

Where E_g (1.79 eV) is the energy gap of CdSe.[3] $E_{emission}$ is calculated in a way which avoids the consideration of the coulomb potential twice (both for the electron and both for the hole). We marked the notation of the levels as $X_{\#l}$ where X can be e (for electron level), hh (heavy hole), lh (light hole) and so (split off). # is number of nodes along the rod axis and l is the symmetry in the perpendicular direction to the rod axis (s, p, d). For example in figure 1 we are plotting the cross-section along the xy plane in the middle of the rod for the 3 electron levels e_{0s}, e_{0p} and e_{0d}.

Since our experimental data is in the range 1.8-2.3eV we need to consider any transition in this range. In Figure S2 we are plotting all the electron (black) and hole (hh red, lh blue and so green) energy levels within 0.5 eV from the lowest energy level for the electron and from the highest level for the hole. On the right we are plotting the wave-functions, the 9 first energy levels of the electron and 3 first energy levels of each kind of hole. In general, we can see that while the electron levels are discrete at least close to the band edge, the hh levels (red) are continuous because of their heavier effective mass and the relatively large dimensions of our NRs. The lh (blue) and so (green) bands have lighter mass thus showing discretization. The electron density of states presented in the main text (Figure 1b) was created by broadening each energy electronic level in figure S2 by a Gaussian with 26 meV width.

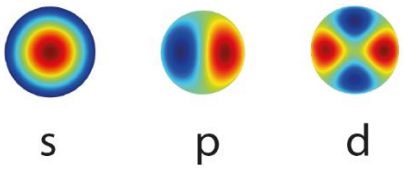

Figure S1. Cross-section for e_{0s}, e_{0p} and e_{0d} electron levels in the middle of the rod.

Table S1. Material parameters used in the simulations.[3,4]

	CdSe	Environment	Units	Ref.
V_c^e	1.79	5+1.79	[eV]	(5)
V_v^{hh}	0	-5	[eV]	(5)
V_v^{lh}	-0.039	-5	[eV]	(5)
V_v^{so}	-0.418	-5	[eV]	(5)
m_e^*	0.112	1	m_0	(6)
$m_{hh\perp}^*$	0.48	1	m_0	(6)
$m_{hh\parallel}^*$	1.19	1	m_0	(6)
m_{lo}^*	0.16	1	m_0	(6)
m_{so}^*	0.12	1	m_0	(6)
$\varepsilon_\perp$	9.29	1	-	(6)
$\varepsilon_\parallel$	10.16	1	-	(6)

The next step is to calculate the oscillator strength for every possible transition within 0.5 eV from the band edge transition. These calculations are presented in figure S3. Every transition from one of the electron levels to the hh levels is marked in red. Every transition from one of the electron levels to the lh levels is marked in blue and every transition from one of the electron levels to the so levels is marked in green.

For the strong transitions we also mark which energy levels are involved in this transition alongside with the wave functions associated with these levels. As a general rule we can see that the selection rule for the transitions is that they have the same symmetry. The electron DOS presented in the main text (Figure 1b) created by broadening each energy electronic level in figure 2 by a Gaussian with 26meV width.

The next step is to calculate the oscillator strength for every possible transition within 0.5 eV from the band edge transition. These calculations are presented in figure S3. Every transition from one of the electron levels to the hh levels is marked in red. Every transition from one of the electron levels to the lh levels is marked in blue and every transition from one of the electron levels to the so levels is marked in green.

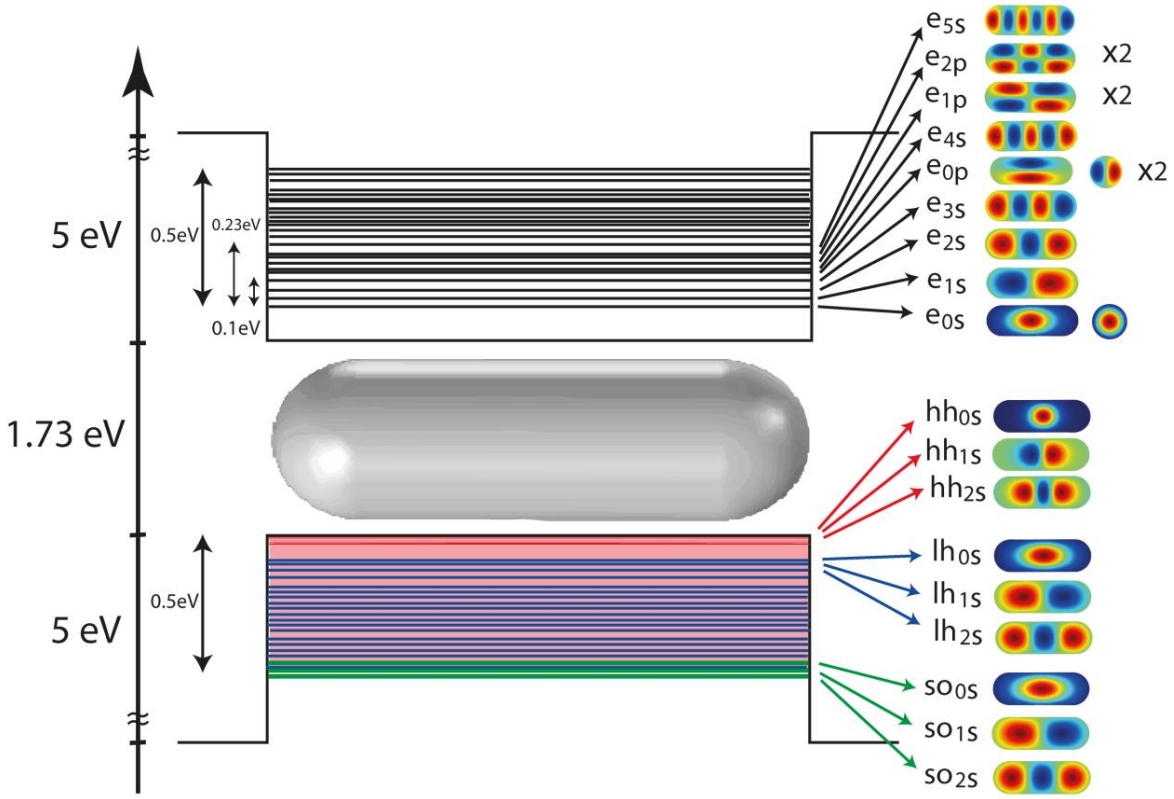

Figure S2. Energy levels of electrons (black) and holes (hh red, lh blue and so green) within 0.5 eV of the lowest energy level for the electron and from the highest level for the hole. The right-hand side shows the wave-functions of the 9 first energy levels of the electron and the 3 first energy levels of each kind of hole.

For the strong transitions we also mark which energy levels are involved in this transition alongside with the wave functions associated with these levels. As a general rule we can see that the selection rule for the transitions is that they have the same symmetry.

Looking at the location of the peaks and comparing them to the experimental data, we can see that the first peak is at 1.82 eV close to the experimental data ~1.85 eV, while the first excitonic peak in which the split off band is involved is at 2.3 eV like the experimental data.

The coupling that we observe experimentally between the ~1.85 eV transition to the 2.3 eV transition is because these two transitions are sharing the same first electron level e_{0s}. As a matter of fact the first transition which involves the lh hole (1.9eV) should also be coupled to these two transitions and indeed in the 2D spectrum there is a broad peak around 1.85 eV probably including both hh and lh transitions. This situation is manifested in Figure S4.

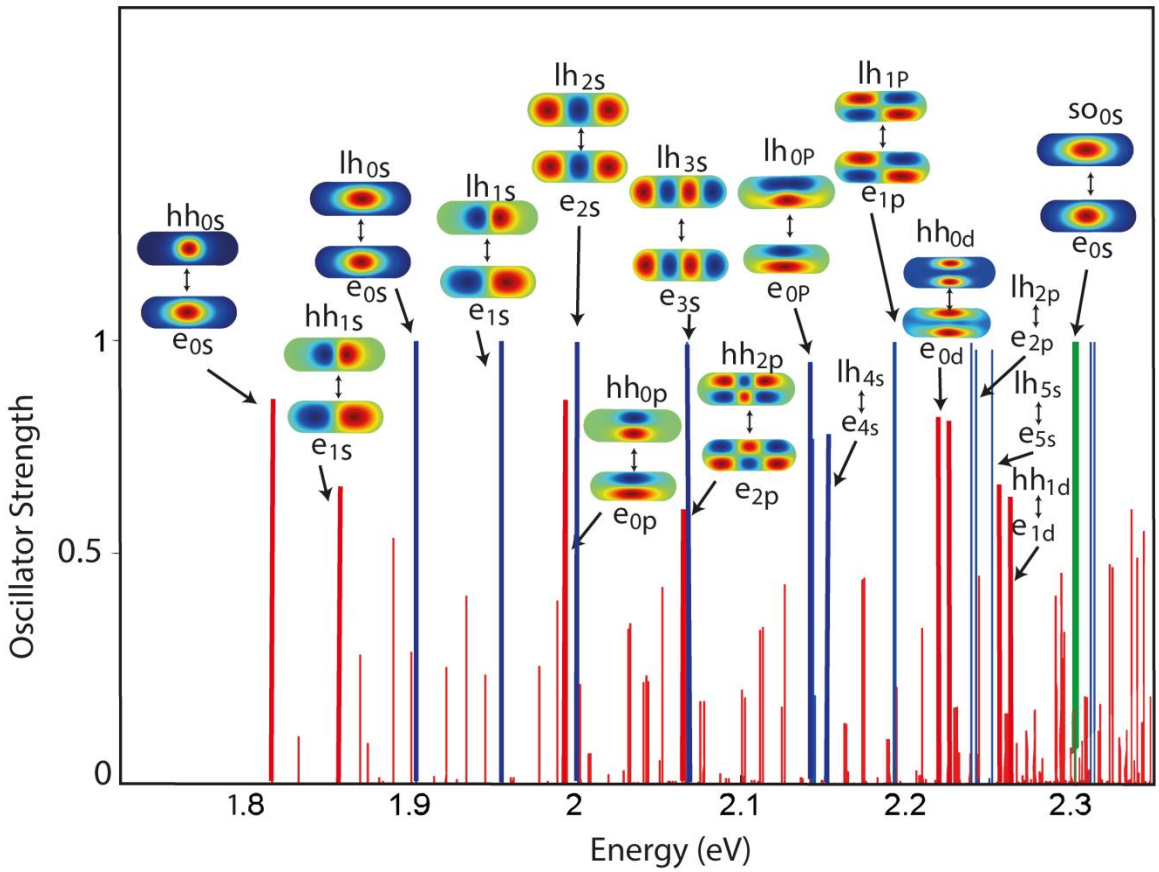

Figure S3. Oscillator strength for every possible transition within 0.5 eV from the band edge transition.

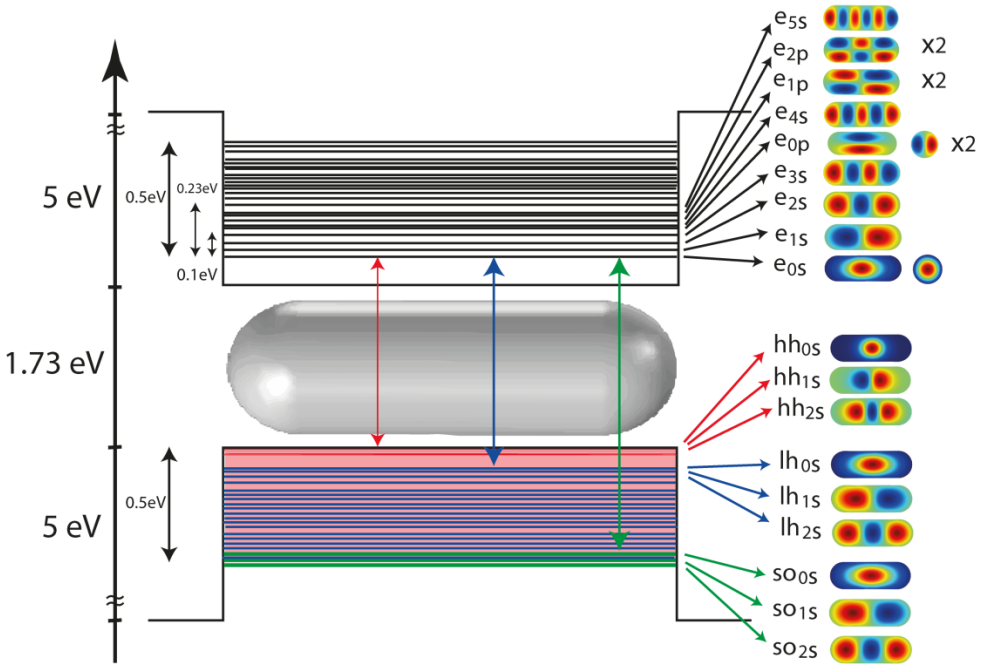

Figure S4. Electronic transitions justifying the presence of a bleach at 2.3 eV following excitation at 1.86 eV.

Ultrafast spectroscopy

The laser source in all ultrafast optical spectroscopy experiments reported here was a 100-fs, 1-kHz repetition rate Ti:sapphire laser system (Libra, Coherent) with a central wavelength of 800 nm (1.55 eV). The broadband ultrashort pulses from Figure 1a in the main text were generated using non-collinear optical parametric amplifiers, as previously described.[5] The sample was placed inside a custom-made cuvette with optical pathlength of 200 μm and windows also of 200 μm. The pulses in the near-infrared were compressed using a prism-pair, while those in the visible were compressed using chirped mirror pairs. The compressed pulses were characterized using second harmonic frequency-resolved optical gating and optimized at the sample position measuring polarization-gated frequency resolved optical gating of the pure solvent inside the cuvette.[6]

The transient absorption (TA) setup allows the use of either NOPA as pump and/or probe. For single color experiments, a thin broadband beamsplitter is used to divide the NOPA output into the pump and probe beams, while a second optical path and removal of the beamsplitter allows either of the NOPAs to be used as pump and/or probe. The time delay between pump and probe is generated using a mechanical delay stage. Measurements are performed in transmission using a SP2150 Acton, Princeton Instruments spectrometer equipped with a CCD detector. The differential transmission ($\Delta T/T$) is acquired as a function of probe wavelength and pump-probe delay.

Two-dimensional electronic spectroscopy

Two-dimensional electronic spectroscopy (2DES) is an extension of broadband transient absorption (TA) with high temporal resolution which addresses its main drawback. High temporal resolution TA requires broadband excitation pulses, and therefore the kinetics observed consist of a superposition of the kinetics coming from the different excitation photon energies contained in the pulse's spectrum. This is a consequence of using a two-pulse experimental method to measure a third-order nonlinear signal, which creates a degeneracy between the first and second field-matter interactions that generate the measured signal, both of which take place with the pump beam.

Two-dimensional spectroscopy addresses this problem by adding a second pump pulse and experimentally controlling the time delay between the pump pulses with interferometric precision, acquiring the nonlinear optical signal as a function of this new delay t_1 for each pump-probe delay t_2. A Fourier transform along the t_1 dimension recovers the excitation energy, yielding a correlation map between excitation and probe photon energies for each pump-probe delay t_2. The techniques can be related by considering that the broadband TA signal is proportional to the integral of the 2DES signal along the pump energy axis. Besides recovering high time resolution kinetics with excitation photon energy specificity, 2DES offers many other advantages with respect to TA, such as distinguishing inhomogeneous from homogeneous line broadening mechanisms, revealing spectral diffusion of inhomogeneous lineshapes, measuring coupling between different bands and coherent oscillations. TA tends to be more convenient when none of these points is needed, as it avoids signal acquisition along an extra dimension, thus yielding higher signal-to-noise ratio for a given measurement time. Many experimental approaches to 2DES exist. Ours relies on a common-path interferometer based on birefringent wedges called TWINS and is described elsewhere.[7,8] The pump pulse is propagated through the wedges, which convert it into two replicas at orthogonal polarizations, and the insertion of the wedges allows us to control the time delay between the replicas. The two replicas are finally projected to a common polarization by a polarizer, and a second set of chirped mirrors is added to account for the extra material added.

Ultrafast relaxation in CdSe nanorods

The CdSe NRs studied here show a broad and convoluted absorption spectrum in which three bands can be distinguished at 1.86 eV, 2 eV and 2.3 eV approximately (see Figure 1a in the main text). The band at 2.3 eV certainly contains contributions from the split-off valence band, which has a characteristic shift of 0.42 eV from the light and heavy hole bands in CdSe.[9] We have applied 2DES to unravel the relaxation pathways across this spectral range. We acquired seventy 2DES maps, with t_2 spanning from -42 fs to 2000 fs, with t_1 ranging from -30 fs to 250 fs; representative 2DES maps are shown in Figure 2a-c in the main text.

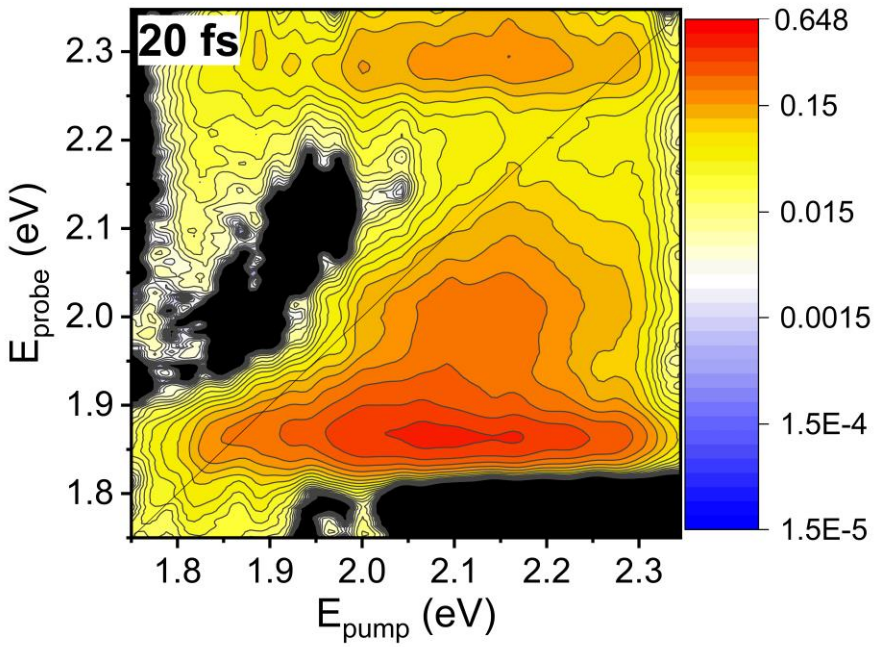

Figure S5. 2DES signal of CdSe NRs at 20 fs (same as Figure 2a), using a logarithmic color scale.

We analyzed the kinetics of all excitation and probe photon energy coordinates in a self-consistent way by employing a global analysis routine that fits the kinetics with a set of exponential components that is common to all coordinates, with only the amplitude being variable among coordinates.[10] We found that two components of 106 fs and 223 fs were sufficient to fit the data, along with one fixed component much longer than the last experimental time delay of 2000 fs. To visualize the amplitude of each exponential component in the 2DES maps we plot in Figure S5 maps containing the amplitude of each component as a function of pump and probe photon energies, which are called 2D decay associated spectra (2D-DAS). A positive 2D-DAS amplitude corresponds to a photobleaching (PB) decay or a photo-induced absorption (PIA) rise, while a negative DAS amplitude corresponds to a rising PB or decaying PIA.

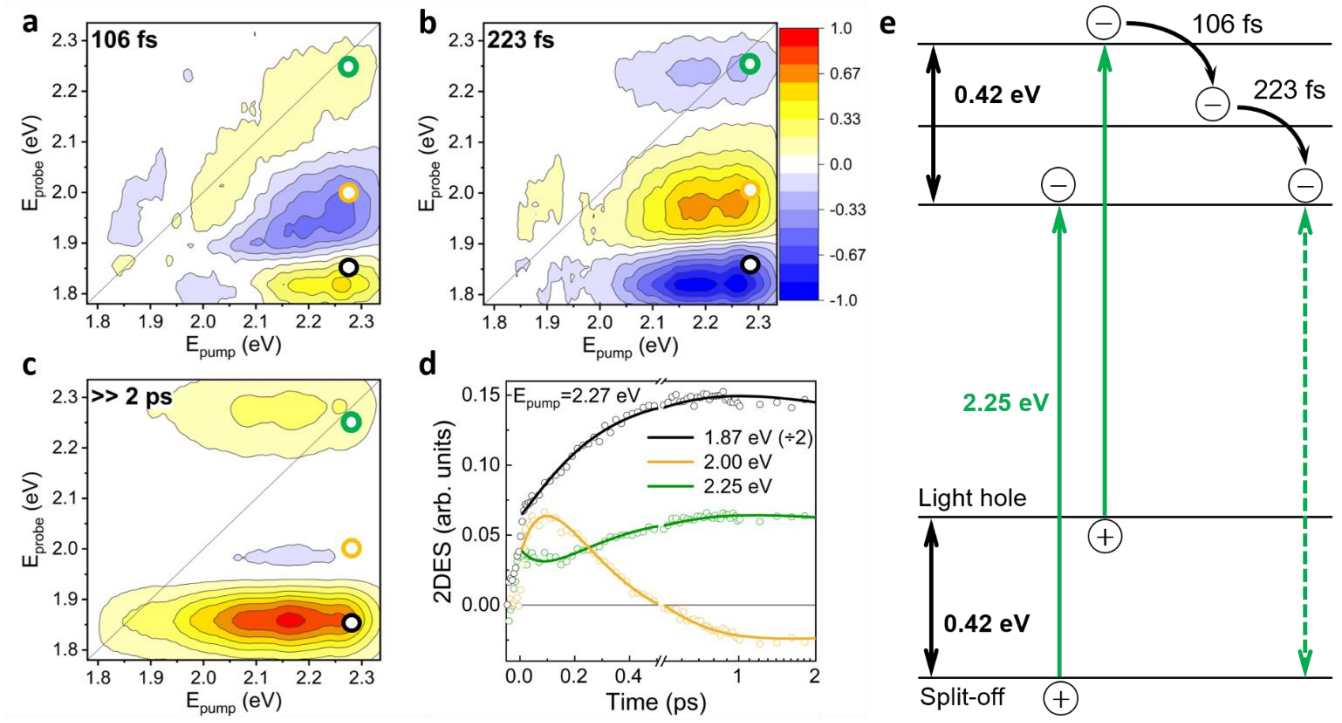

Figure S6. Decay associated spectra corresponding to the three exponential components included in the global fit. (a) 106 fs, (b) 223 fs, and (c) 25 ps, normalized to the maximum value among the three plots. (d) Representative traces comparing data and the fits for pump energy of 2.27 eV and three values of the probe energy. (e) Scheme of the kinetics, explaining the unusual decay and then recovery of the photobleach at the 2.25 eV band.

In Figure S6a we can see that the 106 fs component includes a diagonal decay for pump and probe energies above 1.9 eV. This decay is accompanied by a rising PB at probe energies between 1.9 and 2.05 eV, meaning that the carriers originally at the diagonal at time zero relax to this 1.9 to 2.05 eV region with a 106 fs time constant. Finally, we also observe positive amplitude at probe energies around 1.8 eV, which we assign to a decay of the sub-gap PIA band seen in Figure 2a in the main text, as the now colder carriers no longer shift the bandgap. The amplitudes of the 223 fs component show the second and final step of the relaxation to the bandgap. The carriers that had reached the 1.9-2.05 eV probe range now decay, and a rising amplitude at the bandgap is observed.

Interestingly, we also observe a rising amplitude at probe energies around 2.25 eV. Figure S6d shows that this is a real signal, not an artifact of the fit procedure. We explain this rising signal with the presence of more than one transition around 2.3 eV. Not only is it possible to promote electrons from the split-off valence band to the bottom of the conduction band, but it is also possible to promote electrons from the light and heavy hole valence bands high up into the conduction band, as shown in the scheme in Figure S6e. When the latter relax in 106 fs, some amplitude at 2.3 eV is lost. However, when they finally arrive at the bottom of the conduction band, they add extra bleaching to the split-off valence band, thus increasing the signal at high transition energies.

Complementary transient absorption plots

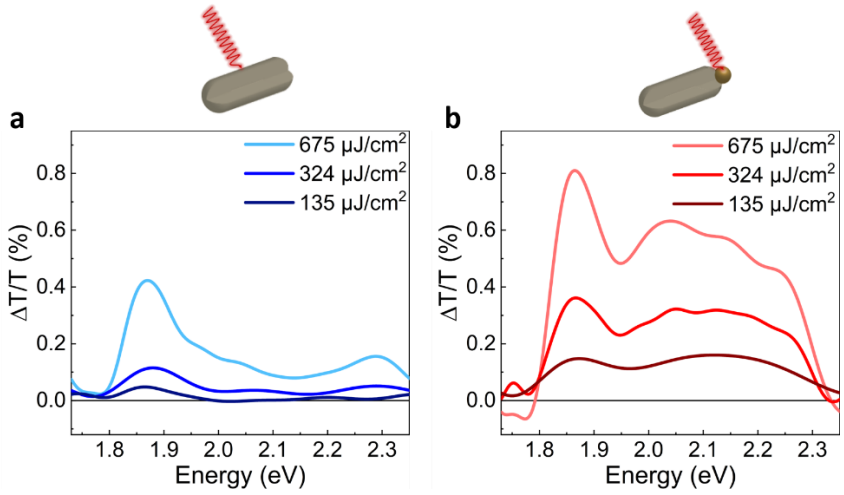

Figure S7. Transient absorption spectra of (a) CdSe NRs and (b) CdSe:Au HNPs samples of the same maximum optical density pumped in the NIR at 300 fs using different fluences. In panel (a) we observe a non-linear growth of the signal, compatible with two-photon excitation of the sample, while in panel (b) we see a linear growth of the signal intensity with the excitation power, showing that even at the highest fluence single photon-excitation dominates. The experiments used in the discussion were performed at the lowest fluence (135 μJ/cm^2).

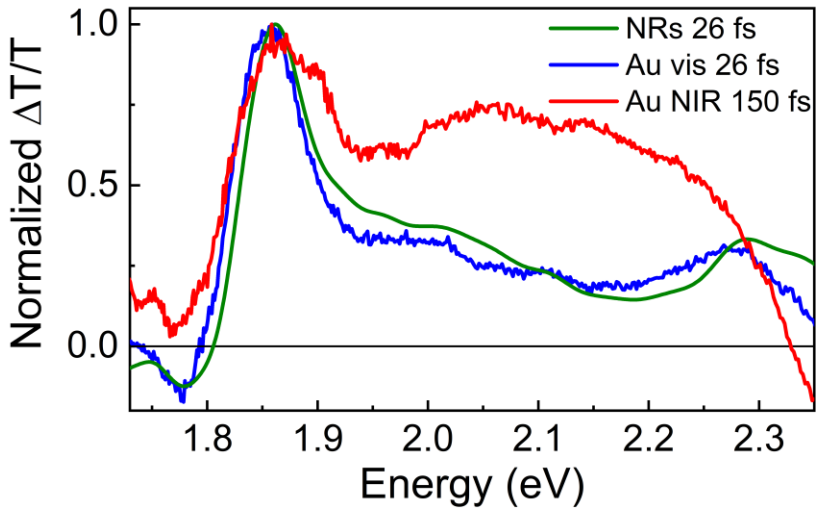

Figure S8. Normalized transient absorption spectra of CdSe NRs and CdSe:Au HNPs pumped in the visible at 26 fs (green and blue, respectively). The red line shows the normalized TA spectrum of the CdSe:Au HNPs 150 fs after NIR photoexcitation.

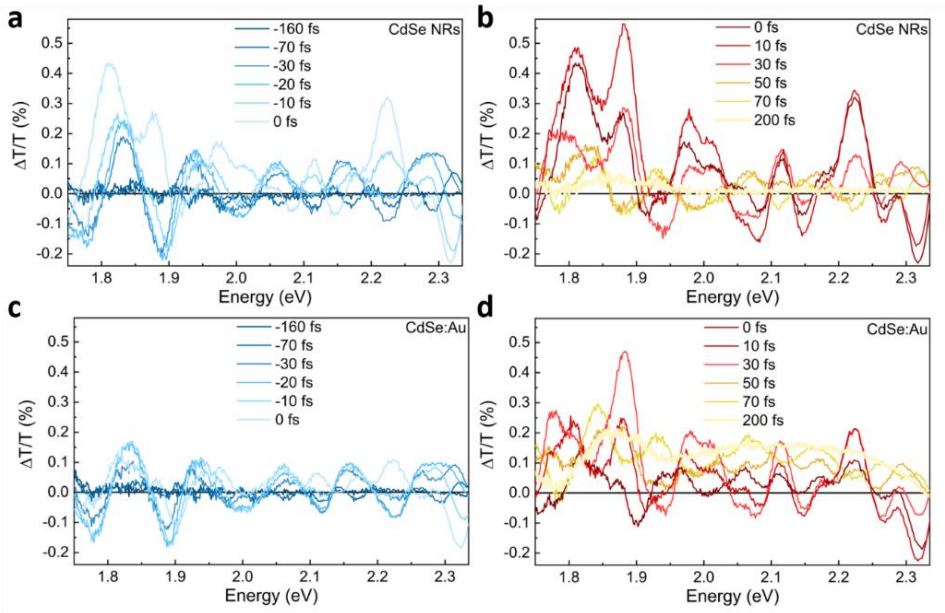

Figure S9. Comparison of cross-phase modulation signatures after broadband pumping at 1.3 eV with 20 nJ per pulse and broadband probing in the visible. (a) and (b) show the signatures observed in bare CdSe NRs at negative (a) and positive (b) times, while (c) and (d) are the same for CdSe:Au HNPs. We note that both vertical and horizontal axes have the same scale. The cross-phase modulation is stronger in the bare CdSe because it has negligible absorption in the spectral range of the pump pulse, whereas CdSe:Au is strongly absorbing in this frequency range. This absorption suppresses cross-phase modulation at the back window of the cuvette and solvent near it. We also note that for bare CdSe NRs the oscillatory features are around a signal level of zero, whereas for CdSe:Au HNPs at positive delays (panel d) the oscillations are observed on top of a positive background, which is the PB signatures from CdSe and gold, thus present from time zero. Finally, the light yellow line in panel (b) shows a bleach at 1.85 eV, due to two photon excitation. Because the hybrid system absorbs significantly at 1.3 eV, unlike the bare NRs, this signal sets an upper limit for CdSe signatures due to two-photon excitation in the HNPs.

TA global analysis

The Global analysis of the TA data was performed using Glotaran, including a Gaussian instrument response function convoluted with the exponential components.[11] Figure S10 shows the DAS obtained for CdSe NRs (Fig. S10a), CdSe-Au HNPs after visible photoexcitation (Fig. S10b) and CdSe-Au HNPs after NIR photoexcitation (Fig. S10c). Similar to the 2DES analysis, a positive DAS represents either adecaying photobleach (PB) or a rising photo-induced absorption (PA). On the other hand, a negative DAS indicates a rising PB or a decaying PA.

The DAS in Fig. S10a reflect the results obtained in Fig. S6, albeit lacking in pump energy resolution, and the timescales are in agreement within experimental errors (120 fs instead of 106 fs for the first component, and 273 fs instead of 223 fs for the second). The 120 fs component in Fig. S10a shows a negative signal peaking at 1.9 eV, corresponding to the rising amplitude of the intermediate transitions. The 273 fs component then includes a positive signal in the 1.9-2.1 eV spectral range, representing a PB decay, while a negative signal is found peaking at around 1.82 eV, which corresponds to the final cooling of the hot carriers generated.

Fig. S10b shows the DAS of CdSe-Au HNPs for visible photo-excitation. The timescale of the first component is similar to that of the CdSe NRs (black dots), but of opposite sign, reflecting the decaying PB from 1.9 to 2.1 eV, corresponding to the hot-electron transfer from CdSe to the gold domain. The bandgap electron transfer can be seen from the positive peak around 1.8 eV in the 212 fs DAS in Fig. S10b (red dots). Finally, the TA signature characteristic of the charge separated states (blue spectrum) is seen to decay in 1.21 ps, leaving only weak thermal signatures behind at longer times (green).

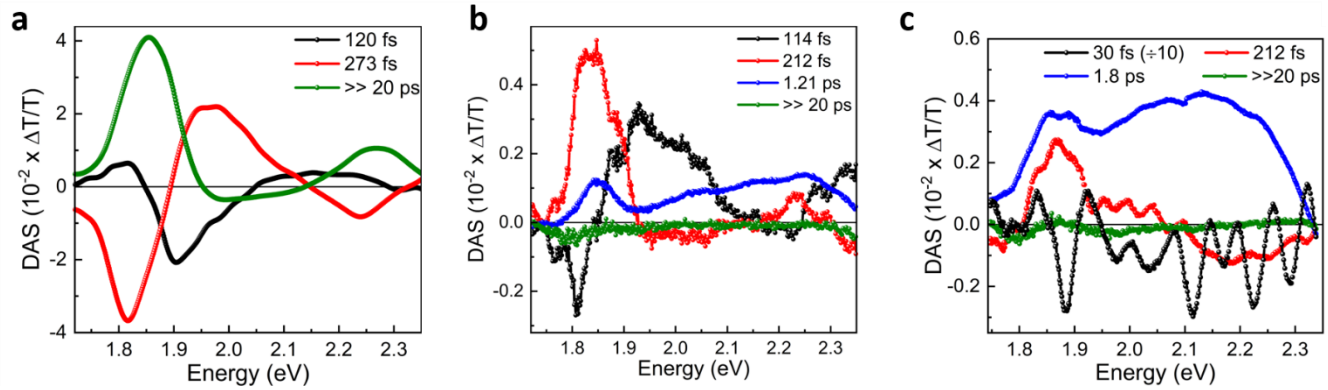

Figure S10. Decay associated spectra corresponding to the TA data from Figure 3 in the main text. (a) CdSe NRs; (b) CdSe-Au HNPs with visible photoexcitation; (c) CdSe-Au HNPs with NIR photoexcitation. All fits included a very long component that is much longer than the experimental time window, which is always shown in green, while black, red and blue stand respectively for the first, second and third (when present) components. The 30 fs component in panel (c) partially captures the cross-phase modulation artifact and was divided by 10 to fit in the same graph.

Fig. S10c shows the DAS for the CdSe-Au HNPs with NIR photoexcitation. The strong 30 fs component (black dots) mostly captures the cross-phase modulation in the two-color experiment, and had its amplitude divided by ten. The second component (red dots in Fig. S10c), at 212 fs shows a decaying PB band centred at 1.85 eV and a rising PB band centred at around 2.2 eV. The decaying PB at 1.85 eV shows a depopulation of electrons from CdSe, and the rising amplitude at 2.2 eV corresponds to the TA associated with the gold, confirming its assignment to the back-transfer of CdSe electrons originally generated via the PICT mechanism. The third component (blue dots) at 1.8 ps reflects cooling of the hot-electrons through electron-phonon coupling in the gold domain, and once again a weak thermal component is left behind, remaining for timescales that greatly exceed our experimental time window.

Table S2: Summary of the global analysis results for the measurements reported.

	τ_1	τ_2	τ_3	τ_4
CdSe NRs 2DES	106 fs	223 fs	>>20 ps	–
CdSe NRs TA	120 fs	273 fs	>>20 ps	–
CdSe-Au vis	114 fs	212 fs	1.21 ps	>>20 ps
CdSe-Au NIR	30 fs	212 fs	1.8 ps	>> 20 ps

References

(1) S. Zhou, L. Dong, S. Popov, A. Friberg, *J. Eur. Opt. Soc.* **2013**, *8*.

(2) C. Grivas, C. Li, P. Andreakou, P. Wang, M. Ding, G. Brambilla, L. Manna, P. Lagoudakis, *Nat. Commun.* **2013**, *4*.

(3) O. Madelung, *Semiconductors Data Handbook*, Springer, Berlin, **2004**.

(4) M. P. Halsall, J. J. Davies, J. E. Nicholls, B. Cockayne, P. J. Wright, *J. Lumin.* **1991**, *48–49*, 735–739.

(5) D. Brida, C. Manzoni, G. Cirmi, M. Marangoni, S. Bonora, P. Villoresi, S. De Silvestri, G. Cerullo, *J. Opt. A Pure Appl. Opt.* **2010**, *12*.

(6) R. Trebino, *Frequency-resolved optical gating: the measurement of ultrashort laser pulses*, Springer, New York, **2000**.

(7) D. Brida, C. Manzoni, G. Cerullo, *Opt. Lett.* **2013**, *37*, 3027–3029.

(8) J. Rehault, M. Maiuri, A. Oriana, G. Cerullo, *Rev. Sci. Instrum.* **2014**, *85*, 123107.

(9) W. Shan, J. J. Song, H. Luo, J. K. Furdyna, *Phys. Rev. B* **1994**, *50*, 8012–8015.

(10) A. Volpato, L. Bolzonello, E. Meneghin, E. Collini, *Opt. Express* **2016**, *24*, 24773–24785.

(11) J. J. Snellenburg, S. Laptenok, R. Seger, K. M. Mullen, I. H. M. van Stokkum, *J. Stat. Softw.* **2012**, *49*, 1–22.